JACS Au
AN OPEN ACCESS JOURNAL OF THE AMERICAN CHEMICAL SOCIETY

pubs.acs.org/jacsau

Article

Ionothermal Access to Defined Oligomers of Supertetrahedral Selenido Germanate Clusters

Zhou Wu, Isabell Nußbruch, Simon Nier, and Stefanie Dehnen*

Cite This: *JACS Au* 2022, 2, 204–213

Read Online

ACCESS | Metrics & More | Article Recommendations | Supporting Information

ABSTRACT: Supertetrahedral chalcogenido (semi)metalate clusters have been in the focus of inorganic and materials chemistry for many years owing to a variety of outstanding physical and chemical properties. However, a critical drawback in the canon of studying corresponding compounds has been the lack of control in assembling the supertetrahedral units, which have been known as either highly charged monomeric cluster anions or lower charged, yet extended anionic substructures of linked clusters. The latter is the reason for the predominance of applications of such materials in heterogeneous environment, or their solubilization by organic shielding, which in turn was unfavorable regarding the optical properties. Recently, we reported a partial alkylation of such clusters, which allowed for a significantly enhanced solubility at a marginal impact on the optical gap. Herein we showcase the formation of finite cluster oligomers of supertetrahedral architectures by ionothermal syntheses. We were successful in generating the unprecedented dimers and tetramers of the $[Ge_4Se_{10}]^{4-}$ anion in salts with imidazolium-based ionic liquid counterions. The oligomers exhibit lower average negative charges and thus reduced electrostatic interactions between anionic clusters and cationic counterions. As a consequence, the salts readily dissolve in common solvents like DMF. Besides, the tetrameric $[Ge_{16}Se_{36}]^{8-}$ anion represents the largest discrete chalcogenide cluster of a group 14 element. We prove that undestroyed cluster oligomers can be transferred into solution by means of electrospray ionization (ESI) mass spectrometry and provide a full set of characteristics of the compounds including crystal structures and optical properties.

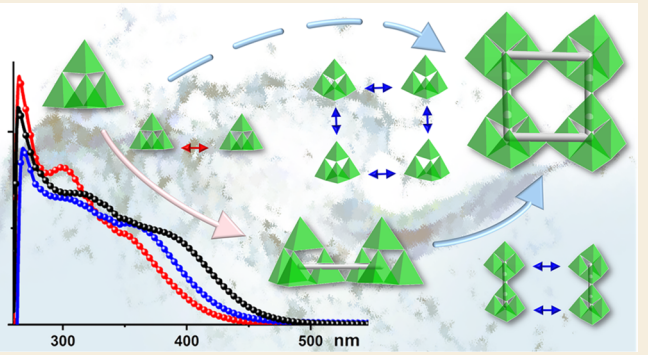

KEYWORDS: *supertetrahedral clusters, atomically precise clusters, semiconductor clusters, cluster oligomers, solubility, optical properties*

1. INTRODUCTION

Atomically precise clusters have been broadly investigated, with the research focus reaching from their designed synthesis to many different fields of application.[1−3] One of the cluster families that has attracted unabated attention to date comprises supertetrahedral chalcogenido (semi)metalate clusters, which stand out owing to their structural beauty but also due to a multitude of fascinating chemical and physical properties.[4−10]

Constant synthetic efforts and analytic methods are applied in this area, and a diversity of structures have been reported. Cluster-based networks gained increasing attention because of the rational integration of porosity and semiconductivity in them.[11] Band gaps that are much narrower than those of zeolites made them ideal candidates for application in photocatalysis and electrocatalysis.[12,13] Corresponding compounds have thus been explored in terms of their use in areas like catalysis,[14] sensing,[15] ion trapping,[16] ion conduction,[17,18] and opto-eletronic devices.[9]

Most of the studies and applications of supertetrahedral clusters so far have been focused on the solid state or suspensions—in many cases owing to the inherently high anionic charges and thus low solubility of salts of discrete (monomeric) clusters on the one hand and the inherent insolubility of one-, two-, or three-dimensional cluster networks in their respective salts on the other hand. Oligomeric assemblies have not yet been realized for purely inorganic clusters. In order to fabricate functional nanomaterials, e.g., for optoelectronic devices, by processing such supertetrahedral clusters, there has been an increasing interest in dissolving such materials in common solvents.[19] However, only a few studies about dissolving ligand-free clusters have been reported, and most of them required the use of highly polar solvents like water or methanol owing to the relatively strong electrostatic interactions between anionic clusters and cationic counterions.[20] Therefore, it is significant and at the same time challenging to alleviate the above-mentioned electrostatic interactions, for a corresponding extension of

Received: October 24, 2021
Published: December 23, 2021

Scheme 1. Schematic Illustration of the Concept of Lowering the Average Charge of Supertetrahedral Chalcogenide Cluster Anions by Formation of Finite Cluster Oligomers

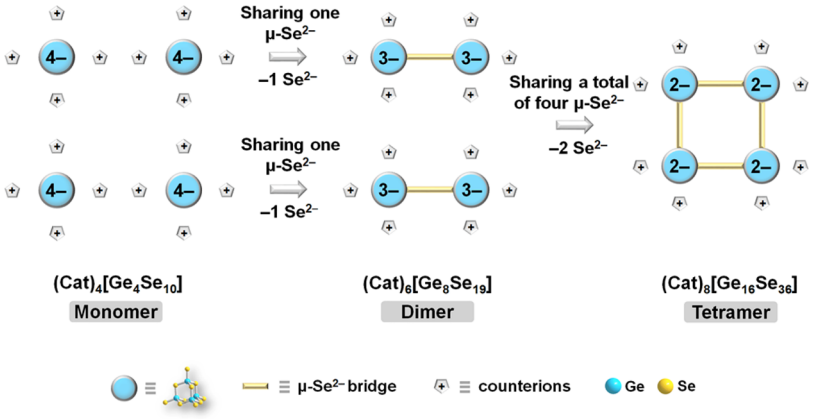

Scheme 2. Summary of the Reactions Yielding Compounds 1−4[a]

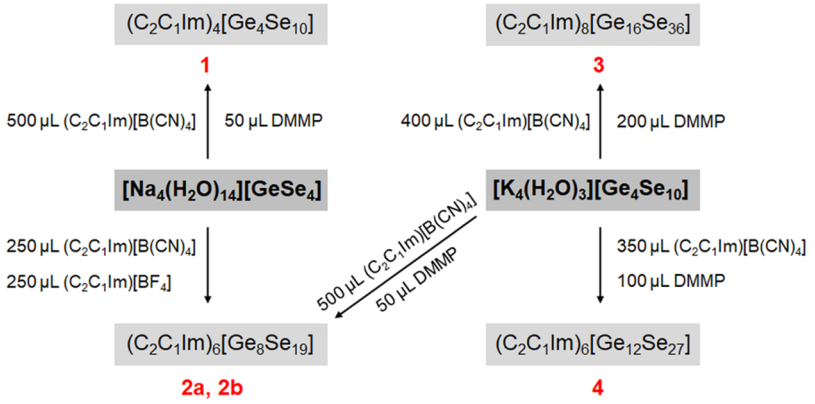

[a]All steps were carried out at 150 °C.

the applications of materials based on supertetrahedral chalcogenido (semi)metalate units. Of course, the solubility of supertetrahedral semiconductor-based clusters is increased if the molecules are fully covered with organic ligands,[21,22] but the organic shielding also leads to widening of the bandgap and quenching of luminescent properties—drawbacks that require new approaches.

One step forward for enhancing solubility is the introduction of ionic liquid counterions, which serves to decrease the lattice energy as long as the charge densities are not too large. Recently, we were able to achieve partial alkylation of the supertetrahedral cluster $[Sn_{10}O_4S_{20}]^{8-}$ in reactive ionic liquids, yielding highly soluble salts of the general composition $(cat)_4[Sn_{10}O_4S_{16}(SBu)_4]$ (cat = imidazolium-based ionic liquid cation).[23] The butyl groups lowered the charge of the clusters (4− instead of 8−) and generated solubility in CH_3CN and CH_2Cl_2, while the optical properties were essentially not affected by the alkyl ligands. However, their attachment to the cluster surface is unfavorable in terms of a limited accessibility of reactive sites. Another recent strategy for slightly enhancing the solubility was realized by introducing a softer chalcogenide ligand: replacement of sulfide with selenide allowed for solubility in DMSO.[6]

As an approach to further increase the solubility of supertetrahedral selenide clusters, we chose to (a) replace alkali metal cations with organic cations in an ionothermal approach and (b) apply conditions that allow a controlled and limited aggregation of the anionic molecules, as an alternative to the generation of (insoluble) extended networks. The assembly of supertetrahedral clusters into oligomers of a finite size, with a corresponding decrease of the average negative charge per cluster unit, has not yet been reported to date.

Herein, we demonstrate the success of this strategy based on a T2-type $[Ge_4Se_{10}]^{4-}$ cluster monomer as a building unit, which was formed in ionic liquids and subsequently condensed into dimers or tetramers (Scheme 1) at distinct compositions of the reaction medium. Key to this was the thorough choice of an adequate relative amount of 2,6-dimethylmorpholine (DMMP) to be added as an auxiliary agent for the connection of chalcogenido germanate units.

In a first step, two of the $[Ge_4Se_{10}]^{4-}$ units form a dimer-like assembly by sharing one of the selenide ligands at the cluster corners as μ-bridges, under release of one Se^{2-} anion per newly formed dimer and a corresponding decrease of the anionic charge per cluster unit. Further condensation of two such dimers yields a tetramer-like assembly by sharing a total of four μ-Se^{2-} ligands upon release of another two Se^{2-} anions. This leads to a significantly lower charge per cluster building unit and a moderate total negative charge of the tetrameric anions. Notably, a certain relative amount of the auxiliary led to the formation of a salt comprising an unprecedented, large zigzag chain as an extended anionic substructure—indicating the necessity of a thorough reaction control for obtaining discrete cluster units.

https://doi.org/10.1021/jacsau.1c00473
JACS Au 2022, 2, 204−213

By following this approach, we not only obtained the first ligand-free chalcogenido (semi)metalate cluster-based dimer and its extension into a square-planar tetramer, $[Ge_{16}Se_{36}]^{8-}$, representing the largest discrete binary chalcogenido (semi)-metalate cluster but also demonstrated that such oligomers readily dissolve in common solvents like dimethylformamide (DMF) without decomposition, which was proven by mass spectrometry and optical absorption spectroscopy of crystals and their solutions.

2. EXPERIMENTAL SECTION

2.1. Syntheses

General Details. All manipulations and reactions were performed in an argon atmosphere by using standard Schlenk or glovebox techniques. $[K_4(H_2O)_3][Ge_4Se_{10}]$[24] and $[Na_4(H_2O)_{14}][GeSe_4]$[25] were synthesized according to literature procedures. 2,6-Dimethylmorpholine (DMMP; Sigma-Aldrich, 99.8%) was dried over P_2O_5, distilled, and stored over a molecular sieve (3 Å). 1-Ethyl-3-methylimidazolium tetracyanoborate, $(C_2C_1Im)[B(CN)_4]$, from Sigma-Aldrich (99.5%) and 1-ethyl-3-methyl-imidazolium tetrafluoroborate, $(C_1C_2Im)[BF_4]$, from Sigma-Aldrich (99.5%) were used as received without further purification.

Variations of the stoichiometric composition of the reactant mixtures led to the formation of a total of five new compounds, as described in the following and summarized in Scheme 2.

Synthesis of $(C_2C_1Im)_4[Ge_4Se_{10}]$ (1). A total of 56 mg (0.077 mmol) of $[Na_4(H_2O)_{14}][GeSe_4]$, 500 μL (2.300 mmol) of $(C_2C_1Im)[B(CN_4)]$, and 50 μL (0.406 mmol) of DMMP were combined in a borosilicate glass ampule, which was sealed airtight thereupon. The ampule was heated to 150 °C at a heating rate of 30 °C/h, kept at 150 °C for 72 h, and then cooled down to room temperature at a cooling rate of 5 °C/h. Pale yellow, needle-like crystals of **1** were obtained in approximately 33% yield.

Synthesis of Two Polymorphs of $(C_2C_1Im)_6[Ge_8Se_{19}]$ (2). **2a**: 40 mg (0.055 mmol) of $[Na_4(H_2O)_3][GeSe_4]$, 250 μL (1.150 mmol) of $(C_2C_1Im)[B(CN_4)]$, and 250 μL (1.616 mmol) of $(C_2C_1Im)[BF_4]$ were combined in a borosilicate glass ampule, which was sealed airtight thereupon. The ampule was heated to 150 °C at a heating rate of 30 °C/h, kept at 150 °C for 72 h, and then cooled down to room temperature at a cooling rate of 5 °C/h. Pale yellow needles of **2a** crystallized in approximately 42% yield. **2b**: 56 mg (0.044 mmol) of $[K_4(H_2O)_3][Ge_4Se_{10}]$, 500 μL (2.300 mmol) of $(C_2C_1Im)[B(CN_4)]$, and 50 μL (0.406 mmol) of DMMP were combined in a borosilicate glass ampule, which was sealed airtight thereupon. The ampule was heated to 150 °C at a heating rate of 30 °C/h, kept at 150 °C for 72 h, and then cooled down to room temperature at a cooling rate of 5 °C/h. Pale yellow needle-like crystals of **2b** were obtained in approximately 2.5% yield. The extremely low yield of this polymorph prevented access to further analytical data beyond the single-crystal structure; therefore, the other approach in the complete absence of DMMP was preferred, and all further data on compound **2** are based on the study of polymorph **2a**, which was accessible in good yield and purity (see above).

Synthesis of $(C_2C_1Im)_8[Ge_{16}Se_{36}]$ (3). A total of 56 mg (0.044 mmol) of $[K_4(H_2O)_3][Ge_4Se_{10}]$, 400 μL (1.840 mmol) of $(C_2C_1Im)[B(CN_4)]$, and 200 μL (1.624 mmol) of DMMP were combined in a borosilicate glass ampule, which was sealed airtight thereupon. The ampule was heated to 150 °C at a heating rate of 30 °C/h, kept at 150 °C for 72 h, and then cooled down to room temperature at a cooling rate of 5 °C/h. Yellow prismatic crystals of **3** were obtained in approximately 26% yield.

Synthesis of $(C_2C_1Im)_6[Ge_{12}Se_{27}]$ (4). A total of 56 mg (0.044 mmol) of $[K_4(H_2O)_3][Ge_4Se_{10}]$, 350 μL (1.610 mmol) of $(C_2C_1Im)[B(CN_4)]$, and 100 μL (0.812 mmol) of DMMP were combined in a borosilicate glass ampule, which was sealed airtight thereupon. The ampule was heated to 150 °C at a heating rate of 30 °C/h, kept at 150 °C for 72 h, and then cooled down to room temperature at a cooling rate of 5 °C/h. Red plate-like crystals of **4** were obtained in approximately 7% yield.

2.2. Single-Crystal X-ray Diffraction (SCXRD)

Single-crystal diffraction data were collected at T = 100 K with Mo Kα radiation (λ = 0.71073 Å) on an area detector system Stoe IPDS-2T (**1**, **3**), on a Bruker D8Quest with a CMOS detector (**2a**), on a Stoe StadiVari diffractometer using Cu Kα radiation (λ = 1.54186 Å) equipped with an Oxford Cryosystems module (**2b**), and on a Stoe StadiVari diffractometer using Ga Kα radiation (λ = 1.34143 Å) (**4**) at T = 150 K. Measurement, structure solution, and refinement results are detailed in Tables S1−S5. Crystallographic data for the structures reported in this paper have been deposited with the Cambridge Crystallographic Data Centre: CCDC-2116247 (**1**), CCDC-2123214 (**2a**), CCDC-2116249 (**2b**), CCDC-2116250 (**3**), and CCDC-2116251 (**4**). Copies of the data can be obtained free of charge upon application to the CCDC (e-mail: deposit@ccdc.cam.ac.uk). Figures were created with Diamond 4.5.[26]

2.3. Powder X-ray Diffraction (PXRD)

PXRD data were obtained with Cu Kα radiation in transmission mode on a Stoe StadiMP diffractometer using a Mythen detector system. The data were examined by using WinXPOW (Figures S7−S9).[27]

2.4. Energy Dispersive X-ray (EDX) Spectroscopy

EDX analyses of single crystals (Figures S11−S14) were carried out using an EDX-device Voyager 4.0 of Noran Instruments coupled with an electron microscope CamScan CS 4DV. Data acquisition was performed with an acceleration voltage of 15 kV and 100 s accumulation time.

2.5. Electrospray Ionization Mass Spectrometry (ESI-MS)

ESI mass spectra were recorded with a Thermo Fisher Scientific Finnigan LTQ-FT spectrometer in negative ion mode. Single crystals of compounds were dissolved in freshly distilled DMF. The solutions were injected into the spectrometer with gastight 250 μL Hamilton syringes by syringe pump infusion. The mass spectra are displayed in Figures S15−S24.

2.6. Dynamic Light Scattering (DLS)

A DynaPro NanoStar device from Wyatt Technology was used for the DLS measurement. Single crystals were dissolved in dry DMF under inert conditions at low concentration. Three drops of the solutions were applied for the study, after equilibration for 1 min at 25 °C in the device prior to the measurements. The Dynals algorithm was used to calculate the size distributions from measured autocorrelation functions;[28] the results are reported as number plots. Three independent measurements were performed on each sample. The curves (Figures S27 and S28) reflect that the obtained R_H values (Table S11) are reliable.

2.7. Raman Spectroscopy

Raman spectra (Figure S29) were recorded on an S&I Mono-Vista CRS+ device with a laser wavelength 633 nm and gratings of 300 and 1200 grooves mm^{-1}. The measurements had a duration of 25 s with 10 coadditions and 10 s with 25 coadditions.

2.8. UV−Visible Spectroscopy

Optical absorption spectra of all compounds (Figure S30) were measured in diffuse-reflectance mode on single crystals and in transmission mode in a fresh solution of the crystals in DMF, employing a Varian Cary 5000 UV/vis/NIR spectrometer from Agilent, equipped with a Praying Mantis accessory for the solid state samples. Tauc plots were generated using the Kubelka−Munk function $(F(R_\infty)h\nu)^{1/\gamma}$, with γ = 0.5, indicative for a direct allowed optical gap.

3. RESULTS AND DISCUSSION

3.1. Syntheses and Crystal Structures

The five title compounds, two of which resemble polymorphs of the same anionic substructure, were synthesized by the

https://doi.org/10.1021/jacsau.1c00473
JACS Au 2022, 2, 204−213

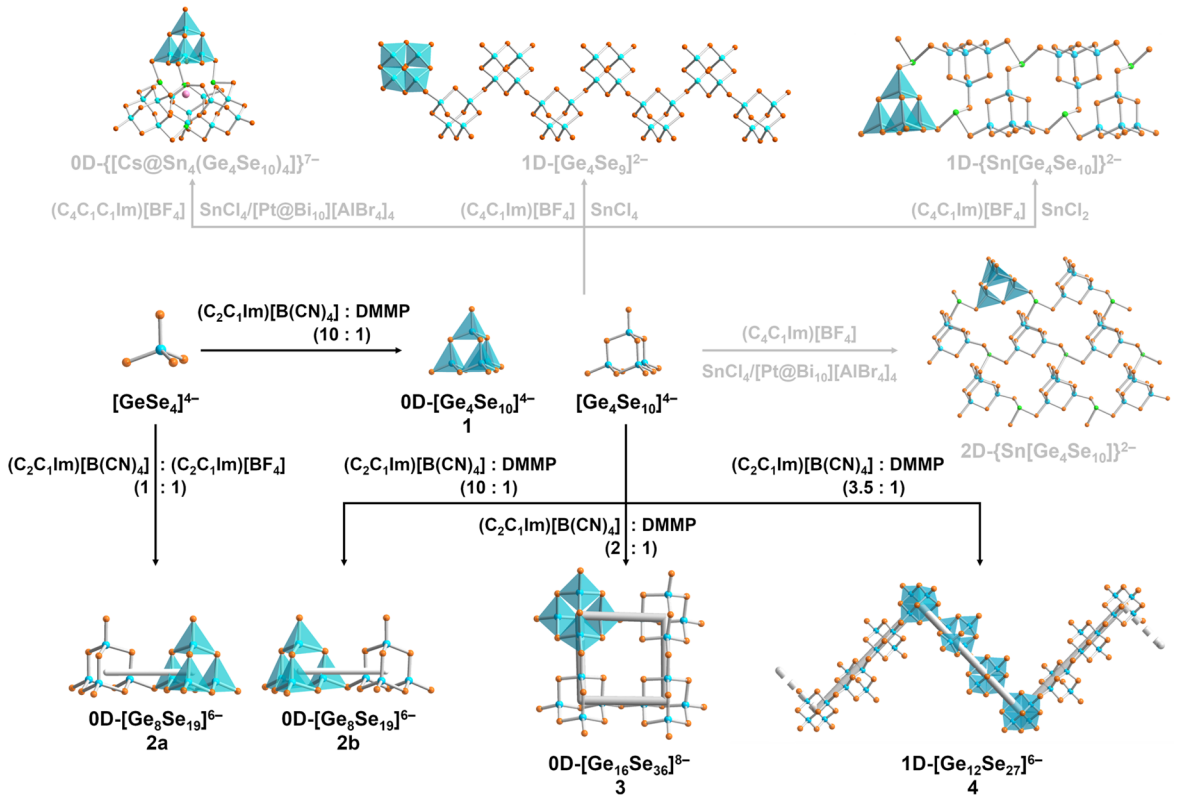

Figure 1. Survey of the formation and use of $[Ge_xSe_y]^{4-}$ anions for the synthesis of more complex anionic substructures in known compounds (top, gray arrows and formulas) and in compounds **1**, **2a**, **2b**, **3**, and **4** reported in this work (center and bottom, black arrows and formulas; all reactions done at 150 °C). Relative amounts are given as v:v ratios. For more details, see the Experimental Section and the Supporting Information. Crystallographically indistinguishable Ge and Se atoms were assigned based on their characteristic coordination modes.

treatment of $[K_4(H_2O)_3][Ge_4Se_{10}]$ in the ionic liquid $(C_2C_1Im)[B(CN_4)]$ and DMMP (**1**, **2b**, **3**, **4**) or by the treatment of $[Na_4(H_2O)_{14}][GeSe_4]$ in a 1:1 mixture of $(C_2C_1Im)[B(CN_4)]$ and $(C_2C_1Im)[BF_4]$ (**2a**) at 150 °C for 3 days. It should be noted that all of the syntheses were sensitive to the reaction temperature: crystals were only obtained upon treatment at 150 °C, while no identifiable compounds were observed at lower (120 °C) or higher (180 °C) reaction temperatures. The most important parameter, however, to be varied for obtaining the different products was the amount of the auxiliary DMMP relative to the amount of ionic liquid used. The results are summarized in Figure 1, in comparison with reported products of similar reactions.

As indicated in Scheme 2 and Figure 1, most of the reactions reported herein were undertaken with $[K_4(H_2O)_3][Ge_4Se_{10}]$. However, we also obtained pale-yellow crystals of a new salt comprising the same discrete $[Ge_4Se_{10}]^{4-}$ anion, $(C_2C_1Im)_6[Ge_4Se_{10}]$ (**1**), by ionothermal treatment of $[Na_4(H_2O)_{14}][GeSe_4]$ in 500 μL of $(C_2C_1Im)[B(CN)_4]$ in the presence of 50 μL of DMMP. Increasing the relative amount of DMMP caused lower yields. The molecular structure of the anion is shown in Figure 2.

Compound **1** crystallizes in the tetragonal crystal system, space group type $P4_2/n$ (No. 86) with two formula units per unit cell (V = 2251.9(5) Å^3; Figure S1). The accessible void space is filled with the ionic liquid counterions. The Ge−(μ-Se) bond lengths (2.3674(12)−2.3771(11) Å) and Ge−$Se_{terminal}$ bond lengths (2.2604(13) Å) are within the range of reported values.[8,24,29−31]

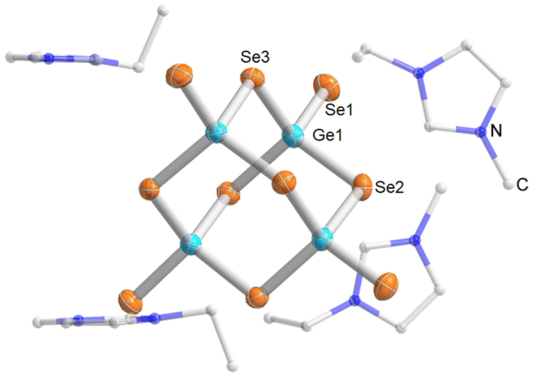

Figure 2. Structure of the anion and four nearest cations in compound **1**. Ge and Se atoms (with atom labeling scheme) are shown as thermal ellipsoids at the 50% probability level; the atoms of the imidazolium counterions are given in wired mode; H atoms are omitted for clarity. Crystallographically indistinguishable Ge and Se atoms were assigned based on their characteristic coordination modes.

By treatment of $[Na_4(H_2O)_{14}][GeSe_4]$ in a mixture of 250 μL of $(C_2C_1Im)[B(CN)_4]$ and 250 μL of $(C_2C_1Im)[BF_4]$ without addition of DMMP, we were able to isolate a dimer of a ligand-free supertetrahedral cluster in $(C_2C_1Im)_6[Ge_8Se_{19}]$ (**2a**). A polymorph of this compound was also generated starting from $[K_4(H_2O)_3][Ge_4Se_{10}]$, by treatment in $(C_2C_1Im)[B(CN)_4]$ in the presence of a very small amount of DMMP (10:1; v:v). The polymorphs **2a** and **2b** crystallize in the triclinic crystal system, space group type $P\bar{1}$ (No. 2, **2a**), and in the monoclinic crystal system, space group type $P2_1/c$

https://doi.org/10.1021/jacsau.1c00473
JACS Au 2022, 2, 204−213

(No. 14, **2b**) with two (**2a**, V = 3735.5(3) Å^3; Figure S2) and four (**2b**, V = 7524.9(9) Å^3; Figure S3) formula units per unit cell, respectively. As shown in Figure 3, two T2 clusters are

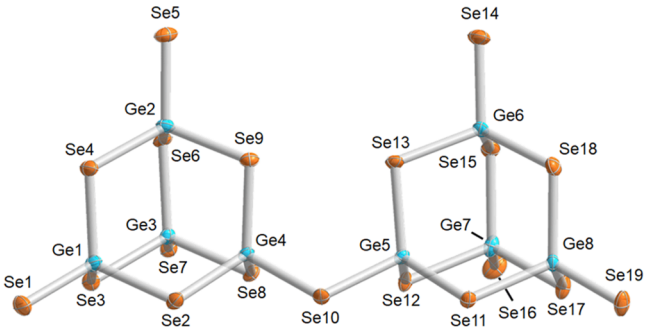

Figure 3. Molecular structure of the anion in compound **2a** (as an example of the very similar anionic structures of **2a** and **2b**) with atom labeling scheme. Ge and Se atoms are shown as thermal ellipsoids at the 50% probability level; imidazolium counterions are omitted for clarity. Crystallographically indistinguishable Ge and Se atoms were assigned based on their characteristic coordination modes.

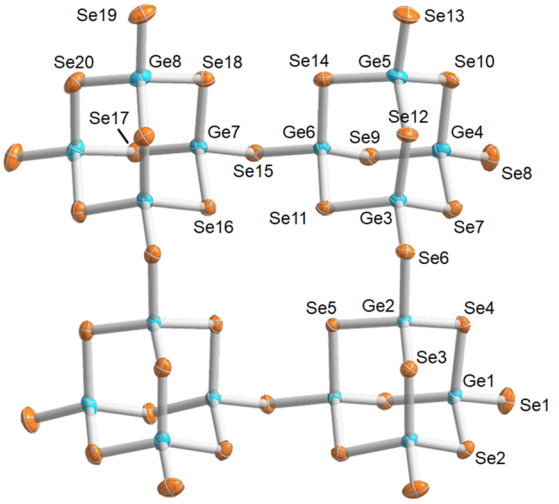

Figure 4. Molecular structure of the anion in compound **3** with atom labeling scheme. Ge and Se atoms are shown as thermal ellipsoids at the 50% probability level; imidazolium counterions are omitted for clarity. Crystallographically indistinguishable Ge and Se atoms were assigned based on their characteristic coordination modes.

linked *via* sharing one μ-Se^{2-} ligand, while three terminal Se^{2-} ligands are retained per building unit. Again, Ge−(μ-Se) bond lengths (2.3296(19)−2.4127(21) Å) and Ge−Se$_{terminal}$ bond lengths (2.2388(21)−2.2640(30) Å) are close to the expected range.[8,24,29−31] Another dimer of supertetrahedral clusters in (DBN-H$^+$)$_6$[In$_{20}$S$_{33}$(DBN)$_6$] has recently been reported.[32,33] However, in this case, six of the terminal cluster positions were occupied by organic substituents, while the dimeric assembly in **2** has a purely inorganic composition.

By significantly increasing the amount DMMP relative to (C_2C_1Im)[B(CN)$_4$] in the reaction mixture used for the preparation of compound **2b**, from 10% to 50% (v:v) and thus the largest relative amount of the auxiliary used in this study, we were able to synthesize (C_2C_1Im)$_8$[Ge$_{16}$Se$_{36}$] (**3**). Compound **3** crystallizes in the monoclinic crystal system, space group type $C2/c$ (No. 15) with four formula units in the unit cell (V = 11596.6(18) Å^3; Figure S4). It comprises an unprecedented tetramer of a chalcogenido (semi)metalate cluster and at the same time the largest discrete and ligand-free binary chalcogenido (semi)metalate cluster; larger species, like the T5-type {In$_{34}$S$_{54}$} moiety,[34] were usually integrated in framework structures so far, and the only known (pseudo)-tetramer of T2-type clusters included linkage by Sn^{2+} ions and inclusion of a Cs$^+$ atom, [Cs@Sn$_4$(Ge$_4$Se$_{10}$)$_4$]$^{7-}$.[8] The molecular structure of the anion in compound **3** is illustrated in Figure 4. Ge−(μ-Se) bond lengths (2.3288(30)−2.3978(33) Å) and Ge−Se$_{terminal}$ bond lengths (2.2296(35)−2.2425(38) Å) match those of the reported ones[8,24,29−31] and also the ones observed in compounds **1** and **2**.

To achieve the unique square-planar structure, one T2 cluster shares two corner Se^{2-} ligands with two neighboring clusters. However, instead of extending their corner-sharing with two further building units, both of the latter T2 units share corners with the same fourth cluster, which closes the macrocycle to form the tetrameric anion. This oligomer of four T2 supertetrahedra can also be regarded as the product of the dimerization of two preformed cluster dimers under release of two additional Se^{2-} anions (see also Scheme 1). This unprecedented assembly of Tn clusters represents the structural alternative to a supertetrahedral arrangement of T2 clusters that would be connected by sharing six (instead of four) corners, thus missing another two Se^{2-} anions and four negative charges. However, a corresponding defect T4-type anion "[Ge$_{16}$Se$_{34}$]$^{4-}$" (or any other group 14−group 16 cluster of this type) has not been described to date. While one may hypothesize that a corresponding structure could form, as it has been known for organometallic chalcogenide clusters, the mismatch of the large size with the low charge has so obviously inhibited its crystallization so far. Indeed, another finite tetrameric assembly of (ternary) supertetrahedral clusters, [Cd$_{16}$In$_{64}$S$_{134}$]$^{44-}$, which was obtained in the ionic compound Cd$_{16}$In$_{64}$S$_{134}$·(DBNH$_2$)$_{11}$(DEMH$_2$)$_{11}$(H$_2$O)$_{50}$ upon solvothermal treatment of Cd(CH$_3$CO$_2$)$_2$·2H$_2$O, In, and S,[10] shows this aggregation pattern but also comprises a much larger charge owing to the presence of di- and trivalent cations instead of tetravalent ones. In this cluster, four {Cd$_4$In$_{16}$S$_{35}$} T4-type units are linked to form a hollow supertetrahedron by sharing six corners.

Another change of the ratio of (C_2C_1Im)[B(CN)$_4$] to DMMP to an intermediate value (3.5:1; v:v) caused the linkage of the [Ge$_4$Se$_{10}$]$^{4-}$ cluster anions *via* μ-Se^{2-} ligands into infinite 1D zigzag chains in (C_2C_1Im)$_6$[Ge$_{12}$Se$_{27}$] (**4**). Compound **4** crystallizes in the monoclinic crystal system, space group type $P2_1/n$ (No. 14). As illustrated in Figure 5 and Figures S5 and S6, the repeat unit of the zigzag arrangement comprises three T2-type building units. These are connected like the three first T2 units in compound **3**, enclosing a near rectangular angle of 95.13°. However, instead of a linkage to the same fourth cluster under formation of the four-membered macrocycle observed in compound **3**, the repeat unit is connected to identical units to both sides, hence extending into an infinite super-zigzag chain with four clusters in a straight row each. This structural motif has also been unprecedented in chalcogenido (semi)metalate chemistry to date.

So far, it has not been possible to gain detailed insight into the processes that lead to the formation of such complex compounds. However, it is obvious that the relative amount of the auxiliary DMMP must play a key role. We assume that the basic molecules serve as mediators for the release of Se^{2-}

https://doi.org/10.1021/jacsau.1c00473
JACS Au 2022, 2, 204−213

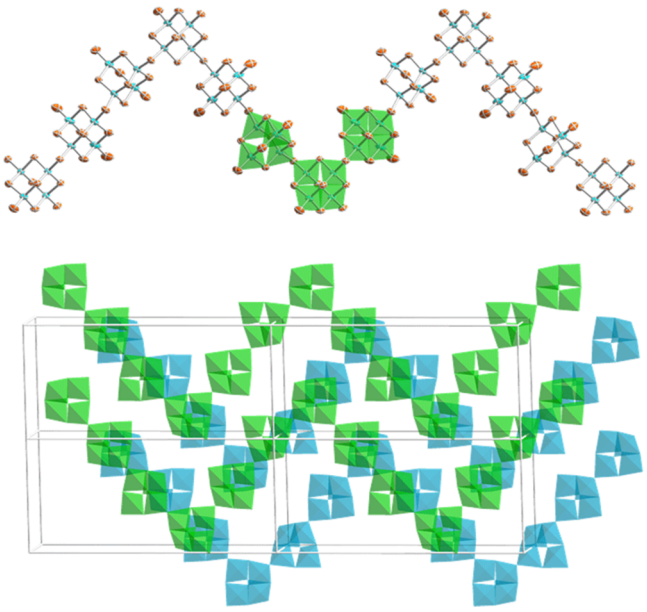

Figure 5. Top: Anionic substructure of compound **4** with atom labeling scheme for the asymmetric unit. Ge and Se atoms are shown as thermal ellipsoids at the 50% probability level; imidazolium counterions are omitted for clarity (for details, see the text). Bottom: arrangement of two anionic zigzag strands in the crystal structure of **4**, accommodated in a 2 × 2 supercell. Crystallographically indistinguishable Ge and Se atoms were assigned based on their characteristic coordination modes.

anions (most probably as H_2Se) upon deprotonation of H_2O (from the reactant) and subsequent hydrogen bonding interactions with the selenido germanate anions. In the presence of a small amount of DMMP (1:10 relative to the ionic liquid), the T1-type $[GeSe_4]^{4-}$ anions assemble to the T2 cluster in **1**, which under the same conditions, if reacted as its K^+ salt, dimerizes to form compound **2**. At a larger relative amount (1:3.5 relative to the ionic liquid), the linkage continues to form the infinite zigzag chains in **4**. In this substructure, all clusters share two corners with adjacent building units. This is also the case for the tetrameric anion in compound **3** that forms at the highest relative amount of DMMP (1:2 relative to the ionic liquid). Hence, besides affecting the mere number of Se^{2-} anions to be released per cluster unit (which is the same as for **4**), the DMMP molecules are supposed to have a more significant templating effect here; we assume that they form H-bonded clusters which control the local tetramerization. We note that all of these assumptions are based on plausibility considerations, as, to this date, there is no reliable method of studying the reactions in situ. The absence of NMR nuclei that allow for quick monitoring and the fact that the reactions take place in sealed ampules during a heating−cooling sequence inhibited corresponding studies. However, we hypothesize that one might get closer to that by means of molecular dynamic simulations one day.

The guest-accessible spaces of all described compounds are filled with counterions to balance the anions' negative charge. While this was fully proven for compound **1**, the assignment of some of the counterions' atoms was inhibited by heavy disorder. In order to avoid impairment of the refinement of the anionic substructures by an incomplete model, the influence of the electron density of atoms that could not be localized from the difference Fourier map was detracted from the data by application of the back Fourier transform method using the SQUEEZE routine in PLATON.[35] The precise Ge:Se ratios were additionally verified by means of EDX spectroscopy (Figures S11−S14). Phase purity was confirmed by PXRD measurement (Figures S7−S9).

As noted above, ligand-free supertetrahedral chalcogenido (semi)metalate clusters have only rarely been assembled into finite cluster oligomers.[8,10] Yet, this might be understood as the very first steps of the formation of extended structures in a bottom-up approach from isolated cluster units—as demonstrated for compounds **1**, **2**, and **4** herein. Hence, we provide the first insights into corresponding materials formation with the example of $[Ge_4Se_{10}]^{4-}$ anions.

As discussed above, this cluster assembly process serves to stepwise lower the charge per cluster unit: from 4− in **1** to 3− in **2** and to 2− in **3** (and **4**; which if the chains were interlinked would ultimately end up with a neutral network of all-corner-linked T2 clusters $[Ge_4Se_6Se_{4/2}]$ in a yet unknown modification of $GeSe_2$). We were therefore eager to investigate the solubility of the crystals comprising molecular anions in a common solvent (DMF) and probe their undecomposed transfer into solution by means of mass spectrometry, UV−visible spectroscopy, and dynamic light scattering experiments. The success of these experiments is documented in the following sections. Compounds **1**−**3** show excellent solubility in dry DMF, determined to be 3.25 mg/mL, 2.75 mg/mL, and 3.13 mg/mL, respectively (1.3 mg of compound **1** in 0.4 mL of DMF; 1.1 mg of compound **1** in 0.4 mL of DMF; 2.5 mg of compound **1** in 0.8 mL of DMF), and they can be dispersed without visible change in other organic solvents and water. We attribute the decent solubility of compound **1**—despite possessing the highest charge per cluster unit—to its selenidic nature and the combination with $(C_2C_1Im)^+$ counterions, both of which lower the lattice energy. These observations discriminate the compounds reported herein from salts of the T5-type supertetrahedral cluster $[Cu_5In_{30}S_{56}H_4]^{13-}$, which only dissolve upon addition of LiBr.[9]

3.2. ESI Mass Spectra

Electrospray ionization mass spectra recorded in negative ion mode, ESI(−), on a fresh DMF solution of single crystals of compound **1** display the signal of the cluster anion along with three counterions. The experimental isotope pattern is in excellent agreement with the calculated isotopic distribution of $\{(C_6N_2H_{11})_3[Ge_4Se_{10}]\}^-$ with a molecular mass of 1414.13 (Figure 6a and overview spectrum in Figure S15). As shown in Figure S16, further monoanionic complexes $\{(C_6N_2H_{11})_2H[Ge_4Se_{10}]\}^-$ and $\{(C_6N_2H_{11})_1H_2[Ge_4Se_{10}]\}^-$ and the aggregate $\{H_3[Ge_4Se_{10}]\}^-$ were transferred into the gas phase. In addition, the signal of $\{(C_6N_2H_{11})_4H[Ge_4Se_{10}]\}^+$ was detected by means of ESI(+) mass spectrometry (Figure S17), which has been unprecedented for a ligand free supertetrahedral chalcogenido (semi)metalate cluster and also is the only ESI(+) signal to be detected among the series of compounds reported herein. This and the identified aggregates—all of which survived the electrospray ionization treatment—confirmed the significant interaction between cluster anions and ionic liquid cations in compound **1**. This is additionally supported by the fact that the mass spectrum of this compound is dominated by molecular peaks with a 1− charge (Figure S15), while this is different for the other compounds reported below.

https://doi.org/10.1021/jacsau.1c00473
JACS Au 2022, 2, 204−213

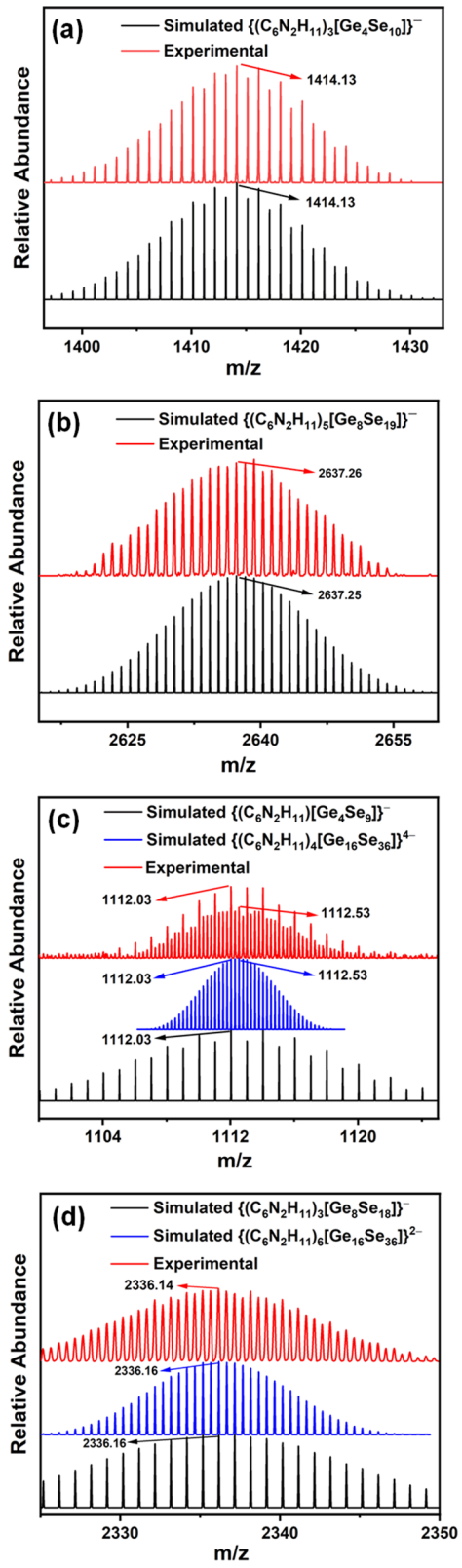

Figure 6. High-resolution ESI(−) mass spectra of the cluster anions in compound **1** (a), compound **2a** (b), and compound **3** (c–d).

For compound **2a**, a series of mass signals referring to monoanionic and dianionic aggregates were observed, in which $(C_2C_1Im)^+$ and H^+ counterions served to decrease the charge. As shown in Figure 6b and in Figures S18 (overview spectrum), S19 and S20, we were able to identify the dimeric cluster anion in compound **2a** along with different quantities of the mentioned cations. Five of them aggregate into monoanions $\{(C_6N_2H_{11})_5[Ge_8Se_{19}]\}^-$, $\{(C_6N_2H_{11})_4H[Ge_8Se_{19}]\}^-$, $\{(C_6N_2H_{11})_3H_2[Ge_8Se_{19}]\}^-$, $\{(C_6N_2H_{11})_2H_3[Ge_8Se_{19}]\}^-$, and $\{(C_6N_2H_{11})_1H_4[Ge_8Se_{19}]\}^-$, and three of the aggregates form dianions, $\{(C_6N_2H_{11})_4[Ge_8Se_{19}]\}^{2-}$, $\{(C_6N_2H_{11})_3H_1[Ge_8Se_{19}]\}^{2-}$, and $\{(C_6N_2H_{11})_2H_2[Ge_8Se_{19}]\}^{2-}$. All of the measured isotope patterns again agree very well with the simulated ones, which indicates a high stability of the species both in solution and in the gas phase. In addition, some fragments were identified, but their relative abundance is significantly smaller than that of the dimeric anions' signals. Most notably, the relative abundance of peaks with 2− charges is larger in this experiment than that in the case of compound **1**. This confirms a reduced cation–anion interaction, as expected and desired owing to the reduced average charge per cluster unit.

For compound **3**, the mass spectra are even more complicated than the spectra of compound **2a**. We observed several series of peaks, with charges from 2− and 3− to 4−. The dominant peaks are found in the range of m/z = 1020 and 1130, and they can be assigned to species with the general composition $\{(C_6N_2H_{11})_{4-x}H_x[Ge_{16}Se_{36}]\}^{4-}$ (x = 0–3). The relative abundance of the species decreases gradually as H^+ replaces the ionic liquid counterions. In addition, cluster anions with a 3− or a 2− charge are detected, but with lower relative abundance than observed for the species with a 4− charge. Notably, no monoanions were observed for solutions of compound **3**, which we attribute both to the large molecular mass and also to an again reduced cation–anion interaction here; this assumption is supported by the described development of relative abundances of species with 4−, 3−, and 2− charges. High-resolution mass spectra for all of these anions are provided in Figure 6c,d and in Figures S21 (overview spectrum) and S22–S24, all of which show excellent agreement of measured and simulated isotope patterns. Again, this is a strong indication for good solubility and fair stability of the compound in DMF. We would like to emphasize that the clusters predominantly dissolve as a whole—in contrast to dispersions of $[Zn_4In_{16}S_{34}]^{14-}$ nanoclusters, for which ESI(−) mass spectra in piperidine indicated the inherent loss of sulfide ligands (along with a massive uptake of H^+).[20] However, some fragmentation was also observed in our studies of compound **3** in the mass spectra, which in part overlays with the molecular peaks of the entire anion. As an example, Figure 6c,d demonstrates the coincidence of $\{(C_6N_2H_{11})_3[Ge_4Se_9]\}^-$ and $\{(C_6N_2H_{11})_6[Ge_{16}Se_{36}]\}^{2-}$ or of $\{(C_6N_2H_{11})_3[Ge_8Se_{18}]\}^-$ and $\{(C_6N_2H_{11})_6[Ge_{16}Se_{36}]\}^{2-}$ (for more details, see the Supporting Information).

In addition, it should be noted that the color of the solutions of all molecular cluster anions remained unchanged over (at least) 4 weeks, indicating their stability under inert conditions (Figure S25a–f). However, the solutions decompose within two hours of exposure to air, as indicated by a color change from yellow to transparent and the precipitation of a black solid (Figures S25g–i).

3.3. Dynamic Light Scattering

The Tyndall effect demonstrated on such solutions (see Figure S26) indicates that the solutes have a nanoparticular dimension. To study this in more detail and to determine the size distribution of the cluster anions in compounds **1**–**3**,

https://doi.org/10.1021/jacsau.1c00473
JACS Au 2022, 2, 204–213

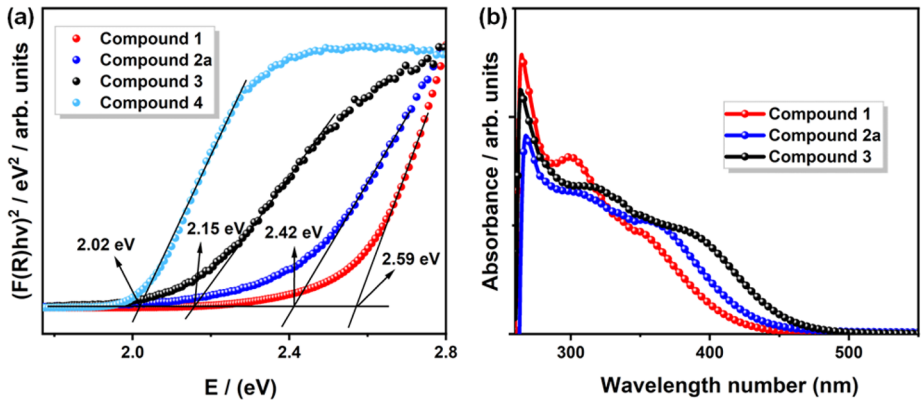

Figure 7. Tauc plots derived from the solid-state UV−visible diffuse-reflectance spectra (Figure S29) of crystalline samples of **1**, **2a**, **3**, and **4** (a) and optical absorption spectrum of fresh solutions of single crystals of **1**, **2a**, or **3** in dry DMF (b).

dynamic light scattering (DLS) studies were carried out on DMF solutions of the single crystals. As shown in Figures S27 and S28, the hydrodynamic radius (R_H) was determined to fall in the ranges of 7.31−8.31 nm (compound **1**), 5.95−8.23 nm (compound **2a**), and 2.93−5.20 nm (compound **3**), respectively (Table S11). The mean diameters of the cluster anions in compounds **1**, **2a**, and **3** (calculated as the largest Se···Se distance plus $2{\cdot}R_{cov}$(Se) = 2·0.116 Å)[36] from the SCXRD analyses are 0.99, 1.70, and 1.90 nm, respectively. This further confirms the notable decrease of the electrostatic interactions between anionic clusters and ionic liquid cations from compound **1** via compound **2a** to compound **3**: Although possessing the largest cluster diameter, compound **3** exhibits the smallest hydrodynamic radius, while the opposite is the case for compound **1**, which shows the largest hydrodynamic radius in spite of its diameter being only 60% of the diameter of compound **2** with a very similar hydrodynamic radius. This is comparable to the effective radii of alkali metal cations in aqueous solutions that decrease from Li^+ to the heavier congeners owing to a significant drop of charge density in this order.[37] In summary, all studies performed on solutions of compounds **1**, **2a**, and **3** confirm (a) the integrity of the cluster assemblies in solution and (b) the notably decreased interaction with counterions (and thus increased solubility) upon oligomerization.

3.4. Vibrational and Optical Absorption Properties

Raman spectra were recorded on single crystals of **1**, **2a**, **3**, and **4**. As illustrated in Figure S29, all spectra exhibit almost identical vibrational modes (although with varied intensities), which indicates the identical bonding situations of these compounds. The most intensive peaks at around 145 cm^{-1}, 217 cm^{-1}, and 339 cm^{-1} are attributed to lattice vibrations of the cluster core, as compared with the reported value of $Na_8Ge_4Se_{10}$,[38] $Na_9Sm(Ge_2Se_6)_2$,[39] $K_2EuGeSe_5$,[40] $Cs_2Ge_3Ga_6Se_{14}$,[41] and $Ge_{24}Se_{76}$.[42] Slight differences are attributed to slight differences of bond lengths or the presence of heteroatoms in the reported cluster cores. The relatively low resolution of the Raman spectra did not allow for the assignment of vibrational bands of the counterions.

UV−visible spectra of crystalline samples (recorded in diffuse-reflectance mode, Figure S30) served to characterize the solid compounds **1**−**4** as narrow-band gap semiconductors. Figure 7a demonstrates a gradual red shift occurs for the lowest excitation energies from **1** to **4**, with the following optical bandgaps being determined by application of the Kubelka−Munk function: 2.59 eV (479 nm; **1**), 2.42 eV (512 nm; **2a**), 2.15 eV (577 nm; **3**), and 2.02 eV (614 nm; **4**). We emphasize here that the optical gaps of all four compounds are narrower than those reported for bulk $GeSe_2$ (2.74 eV)[43] and also for $GeSe_2$ thin films (~1 μm thickness; 2.36 eV),[44] even the ones with molecular selenido germanate anions. This indicates that the cluster-based chromophors are very effective in band gap narrowing.

The absorption spectra recorded on fresh solutions of the crystals in DMF solution (Figure 7b) show a similar red shift, with onsets of absorption at 2.98 eV (416 nm; **1**), 2.88 eV (431 nm; **2a**), and 2.71 eV (457 nm; **3**). The values are blue-shifted by 0.4−0.6 eV relative to the solid samples, but they are still small (in comparison with extended Ge−Se-based solids) given that they stem from molecular anionic units in solution. Notably, the band gap of the dissolved molecular $[Ge_{16}Se_{36}]^{8-}$ anion in **3** is even smaller than that of bulk $GeSe_2$. Owing to its inherent insolubility, it is impossible to record an absorption spectrum of compound **4** in solution.

The investigations demonstrate that although all compounds are based on the same building units (T2 clusters) of the same elements (Ge and Se) and although they even comprise the same counterions, the stepwise oligomerization serves to finely tune the optical gap. This is important with regard to a potential use of such oligomers in functional semiconductor-based arrays.

4. CONCLUSIONS

In summary, a series of narrow-band gap semiconductor clusters are presented that are based on $[Ge_4Se_{10}]^{4-}$ and comprise the first dimers and the first square-shaped tetramer of chalcogenido (semi)metalate supertetrahedra. The compounds were obtained by mild thermal treatment of $[Na_4(H_2O)_{14}][GeSe_4]$ or $[K_4(H_2O)_3][Ge_4Se_{10}]$ in the ionic liquids 1-ethyl-3-methylimidazolium tetracyanoborate, $(C_2C_1Im)[BX_4]$ (X = F, CN), at 150 °C. One of the title compounds is based on the largest selenido germanate cluster anion, $[Ge_{16}Se_{36}]^{8-}$, reported to date. By sharing μ-Se^{2-} ligands, the charge per cluster unit in the oligomeric anions is decreased in comparison to the monomeric clusters, which is reflected in a significantly reduced cation−anion interaction. Consequently, the compounds dissolve readily in DMF, which was demonstrated by means of ESI mass spectrometry and dynamic light scattering studies on corresponding solutions. UV−visible spectra of both the solid compounds and their solutions indicate remarkably small optical band gaps—similar

https://doi.org/10.1021/jacsau.1c00473
JACS Au 2022, 2, 204−213

to that of bulk $GeSe_2$, or even smaller—which are finely tuned with the degree of aggregation. Future studies aim at the expansion of the oligomerization strategy to other supertetrahedral chalcogenido metalate clusters, with the logical next step being the investigation of the related Ge/S system.

■ ASSOCIATED CONTENT

Supporting Information

The Supporting Information is available free of charge at https://pubs.acs.org/doi/10.1021/jacsau.1c00473.

Single-crystal X-ray diffraction (SCXRD) data, supplementary crystallographic figures, powder X-ray diffraction (PXRD) data, light-microscopic images of the single crystals, energy-dispersive X-ray (EDX) spectroscopy, electrospray ionization mass spectrometry (ESI-MS), stability study of solutions of the soluble compounds, dynamic light scattering (DLS), and Raman and optical absorption spectroscopy (PDF)

Crystallographic information file for compound **1** (CIF)

Crystallographic information file for compound **2a** (CIF)

Crystallographic information file for compound **2b** (CIF)

Crystallographic information file for compound **3** (CIF)

Crystallographic information file for compound **4** (CIF)

■ AUTHOR INFORMATION

Corresponding Author

Stefanie Dehnen − *Fachbereich Chemie and Wissenschaftliches Zentrum für Materialwissenschaften, Philipps-Universität Marburg, 35043 Marburg, Germany;* orcid.org/0000-0002-1325-9228; Email: dehnen@chemie.uni-marburg.de

Authors

Zhou Wu − *Fachbereich Chemie and Wissenschaftliches Zentrum für Materialwissenschaften, Philipps-Universität Marburg, 35043 Marburg, Germany*

Isabell Nußbruch − *Fachbereich Chemie and Wissenschaftliches Zentrum für Materialwissenschaften, Philipps-Universität Marburg, 35043 Marburg, Germany*

Simon Nier − *Fachbereich Chemie and Wissenschaftliches Zentrum für Materialwissenschaften, Philipps-Universität Marburg, 35043 Marburg, Germany*

Complete contact information is available at: https://pubs.acs.org/10.1021/jacsau.1c00473

Author Contributions

The manuscript was written through contributions of all authors.

Notes

The authors declare no competing financial interest.

■ ACKNOWLEDGMENTS

The work was financially supported by the German Research Foundation (Deutsche Forschungsgemeinschaft, DFG). Z.W. acknowledges a Ph.D. fellowship from the China Scholarship Council (CSC).

■ REFERENCES

(1) Friedfeld, M. R.; Stein, J. L.; Ritchhart, A.; Cossairt, B. M. Conversion Reactions of Atomically Precise Semiconductor Clusters. *Acc. Chem. Res.* **2018**, *51*, 2803−2810.

(2) Yan, J.; Teo, B. K.; Zheng, N. Surface Chemistry of Atomically Precise Coinage−Metal Nanoclusters: From Structural Control to Surface Reactivity and Catalysis. *Acc. Chem. Res.* **2018**, *51*, 3084−3093.

(3) Wilson, R. J.; Lichtenberger, N.; Weinert, B.; Dehnen, S. Intermetalloid and Heterometallic Clusters Combining p−Block (Semi)Metals with d− or f−Block Metals. *Chem. Rev.* **2019**, *119*, 8506−8554.

(4) Zhang, J.; Bu, X.; Feng, P.; Wu, T. Metal Chalcogenide Supertetrahedral Clusters: Synthetic Control over Assembly, Dispersibility, and Their Functional Applications. *Acc. Chem. Res.* **2020**, *53*, 2261−2272.

(5) Wang, Y.; Zhu, Z.; Sun, Z.; Hu, Q.; Li, J.; Jiang, J.; Huang, X. Discrete Supertetrahedral T5 Selenide Clusters and Their Se/S Solid Solutions: Ionic−Liquid−Assisted Precursor Route Syntheses and Photocatalytic Properties. *Chem. - Eur. J.* **2020**, *26*, 1624−1632.

(6) Hao, M.; Hu, Q.; Zhang, Y.; Luo, M.; Wang, Y.; Hu, B.; Li, J.; Huang, X. Soluble Supertetrahedral Chalcogenido T4 Clusters: High Stability and Enhanced Hydrogen Evolution Activities. *Inorg. Chem.* **2019**, *58*, 5126−5133.

(7) Yang, D.; Li, W.; Xiong, W.; Li, J.; Huang, X. Ionothermal Synthesis of Discrete Supertetrahedral Tn (n = 4, 5) Clusters with Tunable Components, Band Gaps, and Fluorescence Properties. *Dalton Trans.* **2018**, *47*, 5977−5984.

(8) Santner, S.; Wolff, A.; Ruck, M.; Dehnen, S. Multi-Valent Group 14 Chalcogenide Architectures from Ionic Liquids: 0D-{[Cs@$Sn^{II}_4(Ge^{IV}_4Se_{10})_4$]$^{7-}$} and 2D-{[$Sn^{II}(Ge^{IV}_4Se10)$]$^{2-}$}. *Chem. - Eur. J.* **2018**, *24*, 11899−11903.

(9) Li, Z.−Q.; Mo, C.−J.; Guo, Y.; Xu, N.−N.; Zhu, Q.−Y.; Dai, J. Discrete Supertetrahedral CuInS Nanoclusters and Their Application in Fabrication of Cluster-sensitized TiO_2 Photoelectrodes. *J. Mater. Chem. A* **2017**, *5*, 8519−8525.

(10) Li, H.; Kim, J.; O'Keeffe, M.; Yaghi, O. M. $[Cd_{16}In_{64}S_{134}]^{44-}$: 31-Å Tetrahedron with a Large Cavity. *Angew. Chem., Int. Ed.* **2003**, *42*, 1819−1821.

(11) Zheng, N.; Bu, X.; Vu, H.; Feng, P. Open−Framework Chalcogenides as Visible−Light Photocatalysts for Hydrogen Generation from Water. *Angew. Chem., Int. Ed.* **2005**, *44*, 5299−5303.

(12) Benkada, A.; Reinsch, H.; Poschmann, M.; Krahmer, J.; Pienack, N.; Bensch, W. Synthesis and Characterization of a Rare Transition−Metal Oxothiostannate and Investigation of Its Photocatalytic Properties. *Inorg. Chem.* **2019**, *58*, 2354−2362.

(13) Hu, D.; Wang, X.; Chen, X.; Wang, Y.; Hong, A. N.; Zhong, J.; Bu, X.; Feng, P.; Wu, T. S−Doped $Ni(OH)_2$ Nano−electrocatalyst Confined in Semiconductor Zeolite with Enhanced Oxygen Evolution Activity. *J. Mater. Chem. A* **2020**, *8*, 11255−11260.

(14) Hu, D.; Wang, X.; Yang, H.; Liu, D.; Wang, Y.; Guo, J.; Wu, T. Host−guest Electrocatalyst with Cage−confined Cuprous Sulfide Nanoparticles in Etched Chalcogenide Semiconductor Zeolite for Highly Efficient Oxygen Reduction Reaction. *Electrochim. Acta* **2018**, *282*, 877−885.

(15) Zhang, J.; Wang, X.; Lv, J.; Li, D.-S.; Wu, T. A Multivalent Mixed-metal Strategy for Single-Cu^+-ion-bridged Cluster-based Chalcogenide Open Frameworks for Sensitive Nonenzymatic Detection of Glucose. *Chem. Commun.* **2019**, *55*, 6357−6360.

(16) Xiao, C.; Hassanzadeh Fard, Z.; Sarma, D.; Song, T.−B.; Xu, C.; Kanatzidis, M. G. Highly Efficient Separation of Trivalent Minor Actinides by a Layered Metal Sulfide ($KInSn_2S_6$) from Acidic Radioactive Waste. *J. Am. Chem. Soc.* **2017**, *139*, 16494−16497.

(17) Duchardt, M.; Neuberger, S.; Ruschewitz, U.; Krauskopf, T.; Zeier, W. G.; Schmedt auf der Günne, J.; Adams, S.; Roling, B.; Dehnen, S. Superion Conductor $Na_{11.1}Sn_{2.1}P_{0.9}Se_{12}$: Lowering the Activation Barrier of Na^+ Conduction in Quaternary 1−4−5−6 Electrolytes. *Chem. Mater.* **2018**, *30*, 4134−4139.

(18) Duchardt, M.; Ruschewitz, U.; Adams, S.; Dehnen, S.; Roling, B. Vacancy−Controlled Na^+ Superion Conduction in $Na_{11}Sn_2PS_{12}$. *Angew. Chem., Int. Ed.* **2018**, *57*, 1351−1355.
(19) Zhang, Y.; Wang, X.; Hu, D.; Xue, C.; Wang, W.; Yang, H.; Li, D.; Wu, T. Monodisperse Ultrasmall Manganese-Doped Multimetallic Oxysulfide Nanoparticles as Highly Efficient Oxygen Reduction Electrocatalyst. *ACS Appl. Mater. Interfaces* **2018**, *10*, 13413−13424.
(20) Xue, C.; Zhang, L.; Wang, X.; Hu, D.; Wang, X.-L.; Zhang, J.; Zhou, R.; Li, D.-S.; Su, H.; Wu, T. Enhanced Water Dispersibility of Discrete Chalcogenide Nanoclusters with a Sodalite-Net Loose-Packing Pattern in a Crystal Lattice. *Inorg. Chem.* **2020**, *59*, 15587−15594.
(21) Soloviev, V. N.; Eichhöfer, A.; Fenske, D.; Banin, U. Molecular Limit of a Bulk Semiconductor: Size Dependence of the "Band Gap" in CdSe Cluster Molecules. *J. Am. Chem. Soc.* **2000**, *122*, 2673−2674.
(22) Soloviev, V. N.; Eichhöfer, A.; Fenske, D.; Banin, U. Size−Dependent Optical Spectroscopy of a Homologous Series of CdSe Cluster Molecules. *J. Am. Chem. Soc.* **2001**, *123*, 2354−2364.
(23) Peters, B.; Stuhrmann, G.; Mack, F.; Weigend, F.; Dehnen, S. Highly Soluble Supertetrahedra upon Selective Partial Butylation of Chalcogenido Metalate Clusters in Ionic Liquids. *Angew. Chem., Int. Ed.* **2021**, *60*, 17622−17628.
(24) Wachhold, M.; Kanatzidis, M. G. Surfactant−Templated Inorganic Lamellar and Non−Lamellar Hybrid Phases Containing Adamantane $[Ge_4Se_{10}]^{4-}$ Anions. *Chem. Mater.* **2000**, *12*, 2914−2923.
(25) Krebs, B.; Jacobsen, H. J. Darstellung und Struktur von $Na_4GeSe_4{\cdot}14H_2O$. *Z. Anorg. Allg. Chem.* **1976**, *421*, 97−104.
(26) *Diamond - Crystal and Molecular Structure Visualization, Crystal Impact*; Dr. H. Putz & Dr. K. Brandenburg GbR: Kreuzherrenstr. 102, 53227 Bonn, Germany. http://www.crystalimpact.com/diamond.
(27) Eulenstein, A. R.; Bogdanovski, D.; Reinhardt, H.; Miß, V.; Roling, B.; Hampp, N.; Dronskowski, R.; Dehnen, S. $K_2Ge_3As_3$: Fiberlike Crystals of a Narrow-Band-Gap Zintl Phase with a One-Dimensional Substructure $_\infty^1\{(Ge_3As_3)^{2-}\}$. *Chem. Mater.* **2019**, *31*, 8839−8849.
(28) Hassan, P. A.; Rana, S.; Verma, G. Making Sense of Brownian Motion: Colloid Characterization by Dynamic Light Scattering. *Langmuir* **2015**, *31*, 3−12.
(29) Lin, Y.; Massa, W.; Dehnen, S. Controlling the Assembly of Chalcogenide Anions in Ionic Liquids: From Binary Ge/Se through Ternary Ge/Sn/Se to Binary Sn/Se Frameworks. *Chem. - Eur. J.* **2012**, *18*, 13427−13434.
(30) Zhang, F.; Yin, X.-H.; Liu, X.; Zhou, J. Two Novel Adamantane-Like Thio/Selenidogermanates with Complex Cations. *Z. Anorg. Allg. Chem.* **2011**, *637*, 1388−1393.
(31) Ahari, H.; Garcia, A.; Kirkby, S.; Ozin, G. A.; Young, D.; Lough, A. J. Self-assembling Iron and Manganese metal−germanium−selenide Frameworks: $[NMe_4]_2MGe_4Se_{10}$, where M = Fe or Mn. *J. Chem. Soc., Dalton Trans.* **1998**, 2023−2028.
(32) Sun, L.; Zhang, H.-Y.; Zhang, J.; Jia, Y.-J.; Yu, Y.-Z.; Hou, J.-J.; Wang, Y.-X.; Zhang, X.-M. A Quasi-D3-symmetrical Metal Chalcogenide Cluster Constructed by the Corner-sharing of Two T3 Supertetrahedra. *Dalton Trans.* **2020**, *49*, 13958−13961.
(33) Wu, J.; Jin, B.; Wang, X.; Ding, Y.; Wang, X.-L.; Tang, D.; Li, X.; Shu, J.; Li, D.-S.; Lin, Q.; et al. Breakdown of Valence Shell Electron Pair Repulsion Theory in an H-Bond-Stabilized Linear sp-Hybridized Sulfur. *CCS Chem.* **2021**, *3*, 2584−2590.
(34) Wang, C.; Bu, X.; Zheng, N.; Feng, P. Nanocluster with One Missing Core Atom: A Three-Dimensional Hybrid Superlattice Built from Dual-Sized Supertetrahedral Clusters. *J. Am. Chem. Soc.* **2002**, *124*, 10268−10269.
(35) Spek, A. L. PLATON SQUEEZE: A Tool for The Calculation of The Disordered Solvent Contribution to The Calculated Structure Factors. *Acta Crystallogr., Sect. C: Struct. Chem.* **2015**, *71*, 9−18.
(36) Pyykkö, P.; Atsumi, M. Molecular Single-Bond Covalent Radii for Elements 1−118. *Chem. - Eur. J.* **2009**, *15*, 186−197.
(37) Kielland, J. Individual Activity Coefficients of Ions in Aqueous Solutions. *J. Am. Chem. Soc.* **1937**, *59*, 1675−1678.
(38) Choudhury, A.; Strobel, S.; Martin, B. R.; Karst, A. L.; Dorhout, P. K. Synthesis of a Family of Solids through the Building-Block Approach: A Case Study with Ag^+ Substitution in the Ternary Na−Ge−Se System. *Inorg. Chem.* **2007**, *46*, 2017−2027.
(39) Martin, B. R.; Polyakova, L. A.; Dorhout, P. K. Synthesis and Characterization of a Family of Two Related Quaternary Selenides: $Na_8Eu_2(Si_2Se_6)_2$ and $Na_9Sm(Ge_2Se_6)_2$. *J. Alloys Compd.* **2006**, *408−412*, 490−495.
(40) Evenson; Dorhout, P. K. Synthesis and Characterization of Four New Europium Group XIV Chalcogenides: K_2EuTSe_5 and $KEuTS_4$ (T = Si, Ge). *Inorg. Chem.* **2001**, *40*, 2409−2414.
(41) Ma, N.; Xiong, L.; Chen, L.; Wu, L.-M. Vibration Uncoupling of Germanium with Different Valence States Lowers Thermal Conductivity of $Cs_2Ge_3Ga_6Se_{14}$. *Sci. China Mater.* **2019**, *62*, 1788−1797.
(42) Csarnovics, I.; Veres, M.; Nemec, P.; Molnár, S.; Kökényesi, S. Surface Plasmon Enhanced Light-induced Changes in GeSe Amorphous Chalcogenide − Gold Nanostructures. *J. Non Cryst. Solids* **2020**, *6*, 100045.
(43) Yang, Y.; Liu, S.-C.; Yang, W.; Li, Z.; Wang, Y.; Wang, X.; Zhang, S.; Zhang, Y.; Long, M.; Zhang, G.; Xue, D.-J.; Hu, J.-S.; Wan, L.-J. Air-Stable In-Plane Anisotropic $GeSe_2$ for Highly Polarization-Sensitive Photodetection in Short Wave Region. *J. Am. Chem. Soc.* **2018**, *140*, 4150−4156.
(44) Barik, A. R.; Bapna, M.; Drabold, D. A.; Adarsh, K. V. Ultrafast Light Induced Unusually Broad Transient Absorption in the Sub-bandgap Region of $GeSe_2$ Thin Film. *Sci. Rep.* **2015**, *4*, 3686.

https://doi.org/10.1021/jacsau.1c00473
JACS Au 2022, 2, 204−213